IEEE Photonics Journal
An IEEE Photonics Society Publication

The Non-Vortex Inverse Propagation of Energy in a Tightly Focused High-Order Cylindrical Vector Beam

Volume 11, Number 4, August 2019

Sergey S. Stafeev
Victor V. Kotlyar
Anton G. Nalimov
Elena S. Kozlova

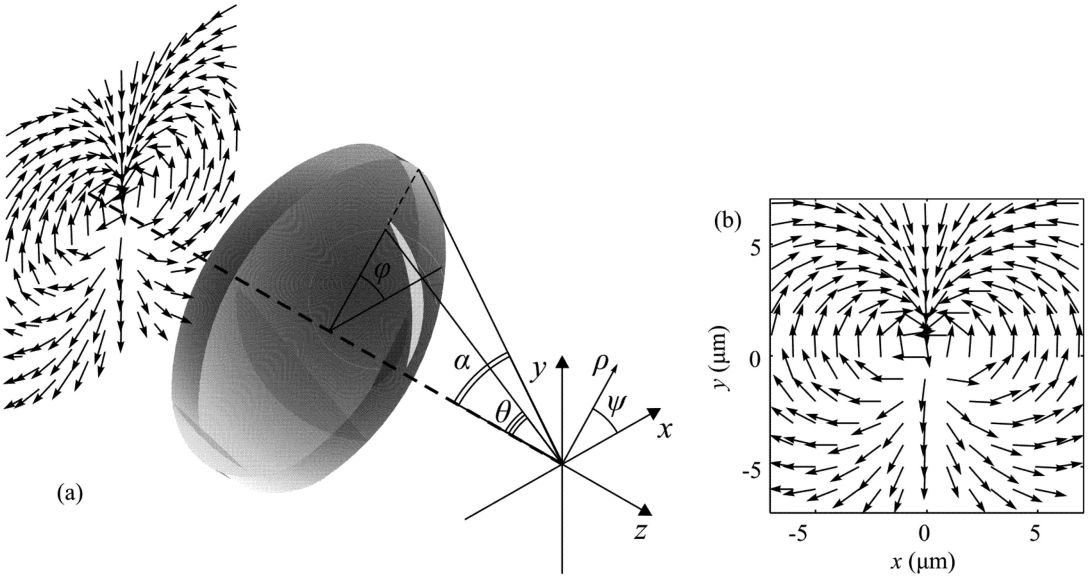

DOI: 10.1109/JPHOT.2019.2921669
1943-0655 © 2019 IEEE

The Non-Vortex Inverse Propagation of Energy in a Tightly Focused High-Order Cylindrical Vector Beam

Sergey S. Stafeev,[1,2] **Victor V. Kotlyar**,[1,2] **Anton G. Nalimov**,[1,2] **and Elena S. Kozlova**[1,2]

[1]Image Processing Systems Institute—Branch of the Federal Scientific Research Centre "Crystallography and Photonics" of the Russian Academy of Sciences, Samara 443001, Russia
[2]Samara National Research University, Samara 443086, Russia

DOI:10.1109/JPHOT.2019.2921669

Manuscript received May 24, 2019; revised May 30, 2019; accepted June 4, 2019. Date of publication June 7, 2019; date of current version July 4, 2019. This work was supported in part by the Russian Science Foundation under Grant 18-19-00595 (in the section "Numerical simulation using Richards-Wolf formulae") by Ministry of Science and Higher Education within the State assignment FSRC "Crystallography and Photonics" RAS under Agreement 007-ГЗ/Ч3363/26 (in the section "Theoretical background"), and in part by the Russian Foundation for Basic Research under Grant 18-07-01122, Grant 18-07-01380, and Grant 18-29-20003 (in the section "Numerical simulation using FDTD-method"). Corresponding author: Sergey S. Stafeev (e-mail: sergey.stafeev@gmail.com).

Abstract: In this paper, the tight focusing of high-order cylindrical vector beams (beams with polarization singularity) was investigated. Using the Richards–Wolf formalism, there were obtained expressions for all projections of the electric and magnetic light fields with *m*-order polarization singularity in the focus of the aplanatic system. Also expressions for the longitudinal component of the Poynting vector were obtained. It was shown that these beams produce in the focal areas with the direction of the Poynting vector opposite to the direction of propagation of the beam. Moreover, the negative values could be comparable in absolute value with positive values; however, this strong inverse energy flow is obtained only while laser light is focused by a lens with high numerical aperture. Of particular interest is the case when the beam order is two ($m = 2$). In this case, the region where the Poynting vector longitudinal projection is negative is located on the optical axis. If the order of the beam is more than two ($m > 2$), than the reverse flow occurs near the optical axis and has a shape of a "tube." Moreover, the width of the negative values region (the diameter of the "tube") increases with increasing order of the beam, however, the absolute value of energy backflow decreases. Earlier, we reported on the observation of a spiral negative energy flow from the center of the focal plane of a focused vortex beam. In this paper, the negative propagation of a laminar near-axis energy flow is reported.

Index Terms: Poynting vector, energy backflow, cylindrical vector beam, tight focusing, Richards-Wolf formulae, FDTD-method.

1. Introduction

Interest in the cylindrical vector beams (CVB), which polarization rotates in the cross-section with the azimuthal angle $0 \le \varphi \le 2\pi$, continues unabated to this day [1]–[6], although they have been investigated in optics for a long time [7]–[11]. Previously researchers have made attempts to generalize cylindrical vector beams by investigating the beams with direction of polarization making several rotations. Such beams in the literature are known as high-order cylindrical vector beams.

For example, the tight focusing of high-order radially polarized modes was investigated in [12]–[16]. These modes had a form of $\mathbf{E}_l(\varphi) = \cos l\varphi \mathbf{i} + \sin l\varphi \mathbf{j}$ where l is the beam order, **i** and **j** are the unit vectors in the Cartesian coordinate system chosen such that the unit vector **k** coincides with the axis of symmetry of the beam. The propagation of higher-order modes with a shifted center was investigated numerically using the Fresnel transform in [17]. The diffraction of higher-order modes by a gap was investigated numerically in [18] also using the Fresnel transform. Experimentally, high-order CVB were early obtained using spatial light modulators [19], [20] and elements designed as Pancharatnam-Berry phase elements [21].

Usually researchers in the field of tight focusing investigate the behavior of the electric component [13]–[16], which makes it impossible to calculate the Poynting vector (PV) in the focal point. According to [22], the direction of scattering force acting on a particle coincides with the Poynting vector. If a beam contains a negative component of PV in its transverse distribution, then the particle illuminated by the beam should move toward the light source. The existence of areas with negative component of PV has been known in optics for a long time (for example, it was obtained by Richards and Wolf in 1959 [23]). However, this negative component was very small usually and only recently it has been possible to obtain focal spots with negative values of PV comparable in absolute value with positive values. For example these beams were obtained in [24], where the propagation of light through the metalens, which simultaneously rotates the direction of polarization and focus the light, was numerically simulated. Using the FDTD method, it was shown that the spiral metalens illuminated by circularly polarized light forms a focal spot with negative values of the energy flow along the propagation axis S_z. The generalization of [24] to the case of focusing of optical vortices with circular polarization and topological charges equal to ± 1, ± 2, and ± 3 was made in [25], [26]. Negative values of the longitudinal component S_z were also obtained in [27], where Gauss-Laguerre beams with circular polarization were investigated, and in [28], where Weber's beams were studied. While the transverse energy flow in a tightly focused azimuthally polarized beam has been discussed [29], the on-axis variations of the Poynting vector were not studied by the authors. As a consequence, the negative propagation of the energy flow was not demonstrated.

In this paper, the tight focusing of high-order cylindrical vector beams (beams with polarization singularity) was investigated. It was shown that these beams produce areas with the Poynting vector direction opposite to the beam propagation direction in the focus. Moreover the negative values could be comparable in absolute value with positive values; however this strong inverse energy flow is obtained only while laser light is focused by a lens with high numerical aperture. Of particular interest is the case when the beam order is two ($m = 2$). In this case, the region where the Poynting vector longitudinal projection is negative is located on the optical axis. If the order of the beam is more than two ($m > 2$), than the reverse flow occurs near the optical axis and has a shape of a "tube". Moreover, the width of the negative values region (the diameter of the "tube") increases with increasing the order of the beam, however the absolute value of energy backflow decreases. In contrast to our previous papers [24]–[26], where the inverse energy flow propagated along a spiral, in this paper we investigate a non-vortex inverse flow with a laminar propagation of light.

2. Theoretical Background

Our analysis relies upon the Richard-Wolf integral: [23]:

$$\mathbf{U}(\rho, \psi, z) = -\frac{if}{\lambda} \int_0^{\alpha} \int_0^{2\pi} B(\theta, \varphi)\, T(\theta)\, \mathbf{P}(\theta, \varphi) \exp\{ik[\rho \sin\theta \cos(\varphi - \psi) + z\cos\theta]\} \sin\theta d\theta\, d\varphi \quad (1)$$

where $\mathbf{U}(\rho, \psi z)$ is the electrical or magnetic field in the focal spot, $B(\theta, \varphi)$ is the incident electrical or magnetic field (θ is the polar angle and φ is the azimuthal angle), $T(\theta)$ is apodization function (for an aplanatic lens the apodization function is equal to $T(\theta) = \cos^{1/2}\theta$ [23], and for the flat diffractive lens it is equal to $T(\theta) = \cos^{-3/2}\theta$ [30]), f is the focal length, $k = 2\pi/\lambda$ is the wavenumber, λ is the wavelength, α is the maximal polar angle determined by the numerical aperture of the lens (NA $=$ $\sin\alpha$), and $\mathbf{P}(\theta, \varphi)$ is the polarization matrix for the electric and magnetic fields. The focusing scheme with the notation for the used variables is shown in Fig. 1a, this approximation is accurate if the

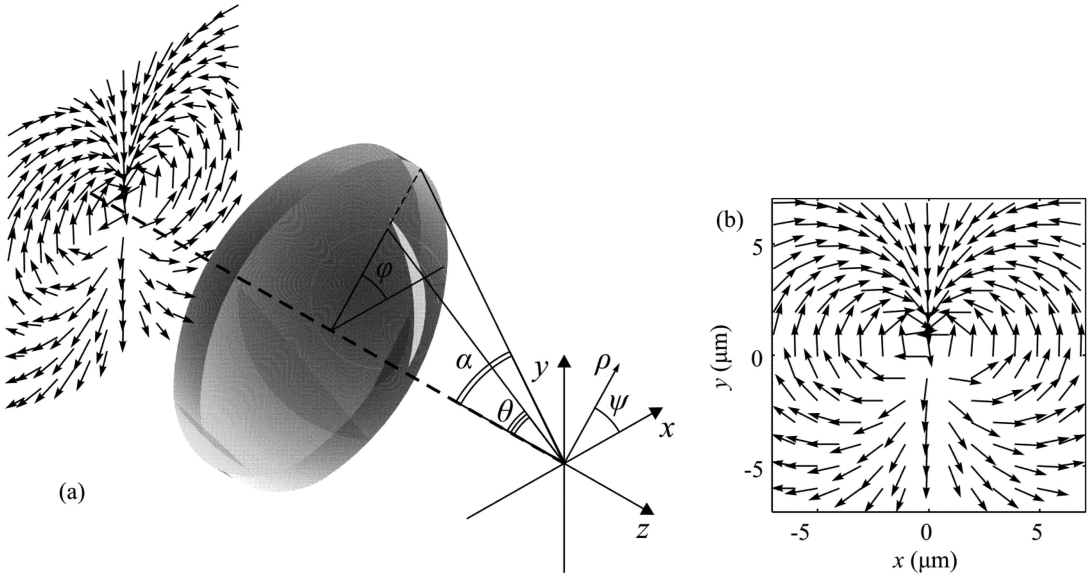

Fig. 1. Focusing scheme (a) and direction of polarization in cylindrical vector beam of the second order $m = 2$ (b).

focal length of the lens is much greater than the wavelength of the incident light. The matrix $\mathbf{P}(\theta, \varphi)$ is equal to:

$$\mathbf{P}(\theta,\varphi) = \begin{bmatrix} 1 + \cos^2\varphi(\cos\theta - 1) \\ \sin\varphi\cos\varphi(\cos\theta - 1) \\ -\sin\theta\cos\varphi \end{bmatrix} a(\theta,\varphi) + \begin{bmatrix} \sin\varphi\cos\varphi(\cos\theta - 1) \\ 1 + \sin^2\varphi(\cos\theta - 1) \\ -\sin\theta\sin\varphi \end{bmatrix} b(\theta,\varphi) \tag{2}$$

where $a(\theta, \varphi)$ and $b(\theta, \varphi)$ are polarization functions for the x- and y- components of the incident beam. For high-order cylindrical vector beams, the polarization functions have the form:

$$E(\theta,\phi) = \begin{pmatrix} a(\theta,\phi) \\ b(\theta,\phi) \end{pmatrix} = \begin{pmatrix} -\sin(m\phi) \\ \cos(m\phi) \end{pmatrix} \tag{3}$$

for the electric field, and

$$H(\theta,\phi) = \begin{pmatrix} a(\theta,\phi) \\ b(\theta,\phi) \end{pmatrix} = \begin{pmatrix} -\cos(m\phi) \\ -\sin(m\phi) \end{pmatrix} \tag{4}$$

for the magnetic field, where m is a positive integer number. If $m = 1$ Eqs. (3) and (4) describe the well known azimuthally polarized beam.

Substituting formulae (3) and (4) into (1), and taking into account (2), we can obtain all six projections of the electric and magnetic field vectors in the focal region of the aplanatic system (the apodization function has a form $T(\theta) = \cos^{1/2}\theta$ [23]):

$$\begin{aligned} E_x &= i^{m+1}[\sin m\varphi I_{0,m} + \sin(m-2)\varphi I_{2,m-2}], \\ E_y &= i^{m+1}[-\cos m\varphi I_{0,m} + \cos(m-2)\varphi I_{2,m-2}], \\ E_z &= -2i^m \sin(m-1)\varphi I_{1,m-1}, \\ H_x &= i^{m+1}[\cos m\varphi I_{0,m} + \cos(m-2)\varphi I_{2,m-2}], \\ H_y &= i^{m+1}[\sin m\varphi I_{0,m} - \sin(m-2)\varphi I_{2,m-2}], \\ H_y &= -2i^m \cos(m-1)\varphi I_{1,m-1}, \end{aligned} \tag{5}$$

where

$$I_{0,m} = \frac{\pi f}{\lambda}\int_0^{\alpha} \sin\ \theta \cos^{1/2}\theta(1+\cos\theta)A_m(\theta)e^{jkz\cos\theta}J_m(x)d\theta,$$
$$I_{2,m-2} = \frac{\pi f}{\lambda}\int_0^{\alpha} \sin\theta\cos^{1/2}\theta(1-\cos\theta)A_m(\theta)e^{jkz\cos\theta}J_{m-2}(x)d\theta,$$
$$I_{1,m-1} = \frac{\pi f}{\lambda}\int_0^{\alpha} \sin^2\theta\cos^{1/2}\theta A_m(\theta)e^{jkz\cos\theta}J_{m-1}(x)d\theta. \quad (6)$$

In (6), $x = kr\sin\theta$, $J_m(x)$ is the m-th order Bessel function, $A_m(\theta) = B(\theta, \varphi)$ is a real function describing the amplitude of the input field in the plane of the entrance pupil of the aplanatic system. It depends only on the angle θ and the order m of the polarization singularity.

From (5), we obtain equations for the components of the electric and magnetic field in the cylindrical coordinate system:

$$E_r = i^{m+1}\sin(m-1)\varphi\,[I_{0,m} + I_{2,m-2}],$$
$$E_\varphi = i^{m+1}\cos(m-1)\varphi\,[-I_{0,m} + I_{2,m-2}],$$
$$E_z = -2i^m\sin(m-1)\varphi\, I_{1,m-1},$$
$$H_r = i^{m+1}\cos(m-1)\varphi\,[I_{0,m} + I_{2,m-2}],$$
$$H_\varphi = i^{m+1}\sin(m-1)\varphi\,[I_{0,m} - I_{2,m-2}],$$
$$H_y = -2i^m\cos(m-1)\varphi\, I_{1,m-1}. \quad (7)$$

From (7), for $m = 1$ follow the well-known expressions for the components of an azimuthally field [11]

$$E_\varphi = I_{0,1} - I_{2,-1} = \frac{2\pi f}{\lambda}\int_0^{\alpha} \sin\theta\cos^{1/2}\theta A_1(\theta)J_1(x)d\theta,$$
$$H_r = -[I_{0,1} + I_{2,-1}] = -\frac{2\pi f}{\lambda}\int_0^{\alpha} \sin\theta\cos^{3/2}\theta A_1(\theta)J_1(x)d\theta,$$
$$H_z = -2iI_{1,0} = -\frac{2i\pi f}{\lambda}\int_0^{\alpha} \sin^2\theta\cos^{1/2}\theta A_1(\theta)J_0(x)d\theta. \quad (8)$$

In particular, from the first equation in (8), it follows that in the focus of the azimuthally polarized beam on the optical axis ($r = 0$), the intensity is equal to zero because $J_1(x) = 0$ for $x = 0$.

From (7), we obtain an equation for the intensity of the electric field in the focal plane $z = 0$:

$$I_m = |E_x|^2 + |E_y|^2 + |E_z|^2 = I_{0,m}^2 + I_{2,m-2}^2 - 2I_{0,m}I_{2,m-2}\cos[2(m-1)\varphi] + 4\sin^2(m-1)\varphi I_{1,m-1}^2 \quad (9)$$

From (9) it could be seen that for $m > 1$, the intensity in the focus is not radially symmetric. From (9) it follows that only for the azimuthal polarization at $m = 1$, the intensity in the focus has the shape of a symmetrical ring:

$$I_1 = (I_{0,1} - I_{2,-1})^2 \quad (10)$$

From (5) we can obtain a simple equation for the longitudinal projection of the Poynting vector [23]:

$$S_z = \frac{1}{2}\mathrm{Re}\left[(\mathbf{E}\times\mathbf{H}^*)_z\right] = \frac{1}{2}\mathrm{Re}\left(E_xH_y^* - E_yH_x^*\right) \quad (11)$$

In the focal plane ($z = 0$), it is equal to:

$$S_{z,m} = I_{0,m}^2 - I_{2,m-2}^2 \quad (12)$$

From (12), it follows that for any m the longitudinal component of PV in the focal plane has circular symmetry relative to the optical axis. This is a strange result because the intensity distribution in the focal plane (9) does not have circular symmetry for $m > 1$. From (12) for $m = 2$, it follows that in the focal plane on the optical axis there is a reverse light energy flow (for any real amplitude in the plane of the entrance pupil $A_2(\theta)$):

$$S_{z,2}(r = 0, z) = -\left(\frac{\pi f}{\lambda}\int_0^{\alpha} \sin\theta \cos^{1/2}\theta(1 - \cos\theta)A_2(\theta)d\theta\right)^2 \tag{13}$$

From (12), it also follows that for $m = 3$ on the optical axis in the focal plane, the energy flow is zero ($S_z = 0$), and in the vicinity of the optical axis it increases quadratically in magnitude with the distance from the axis:

$$S_{z,3}(r \to 0, z) = -\frac{(kr)^2}{4}\left(\frac{\pi f}{\lambda}\int_0^{\alpha} \sin^2\theta \cos^{1/2}\theta(1 - \cos\theta)A_3(\theta)d\theta\right)^2 \tag{14}$$

It should be noted that if in the previous formulae, the apodization function $T(\theta) = \cos^{1/2}\theta$ will be replaced by any other real function; for example, when the apodization function of the diffraction lens $T(\theta) = \cos^{-3/2}\theta$ [30], Eqs. (13) and (14), which prove the existence of an inverse energy flow, will not change. Only a certain value of the integrals in (13) and (14) will be changed. It also should be noted that the existence of the inverse energy flow in the focus of the aplanatic system for $m = 2, 3$ will be obtained for any real function $T(\theta)$.

3. Numerical Simulation Using Richards-Wolf Formulae

In this study, two different numerical methods for simulations were used: the Richards-Wolf integral (1) implemented in MATLAB and FDTD-method implemented in the FullWAVE package. (https://www.synopsys.com/optical-solutions/rsoft/passive-device-fullwave.html).

Figure 1b shows the direction of polarization in the investigated beam of order $m = 2$. In the simulation it was assumed that the zone plate ($T(\theta) = \cos^{-3/2}\theta$ [30], NA = 0.95) focuses the plane wave $B(\theta, \varphi) = 1$. The longitudinal component of PV was calculated using (11), the intensity was calculated as $I = (\mathbf{EE}^*)$, where $\mathbf{E}$ is the electric field.

The results of focusing the second-order ($m = 2$) cylindrical vector beam are shown in Figs. 2–4. Fig. 2a shows the intensity distribution $I = I_x + I_y + I_z$ in the focus. From Fig. 2a, it could be seen that the intensity distribution has the shape of an asymmetrical ring. The asymmetry is explained by the redistribution of energy between components of the electric field due to tight focusing (Fig. 2b-2d). The same effect was shown previously in [12]–[16].

The distribution of the longitudinal component of the Poynting vector S_z in the focal plane is presented in Figs. 3–4. Fig. 3 shows the distribution of S_z in the transverse plane (xy), and Fig. 4 shows the distribution in the longitudinal plane (zy) along the propagation axis of the beam (z-axis). Arrows in Fig. 4 indicate the direction of the Poynting vector without regard to its absolute value.

It is interesting that, in contrast to the focusing of a vortex beam with circular polarization in [24]–[26], in this case there are no transverse components of the Poynting vector S_x and S_y in the focal plane. It means, that the propagation of the energy flow is non-vortex.

It is important to note that the energy backflow comparable to the direct energy flow is observed only in the case of tight focusing. Fig 5 shows the dependence of the minimum value of S_z at the center of the focal spot on the numerical aperture NA for a cylindrical vector beam of the order $m = 2$. From Fig. 5, it could be seen that negative values of S_z are obtained only for large numerical apertures (NA > 0.8).

4. Focusing of CVB With Orders m > 2

In this section, the focusing of CVB with orders greater than m > 2 is considered (Fig. 6 and 7). The intensity distribution and the longitudinal component of the Poynting vector in the focal plane is presented in Fig. 6. Fig. 7a, b show the cross-section of the projection of the Poynting vector S_z

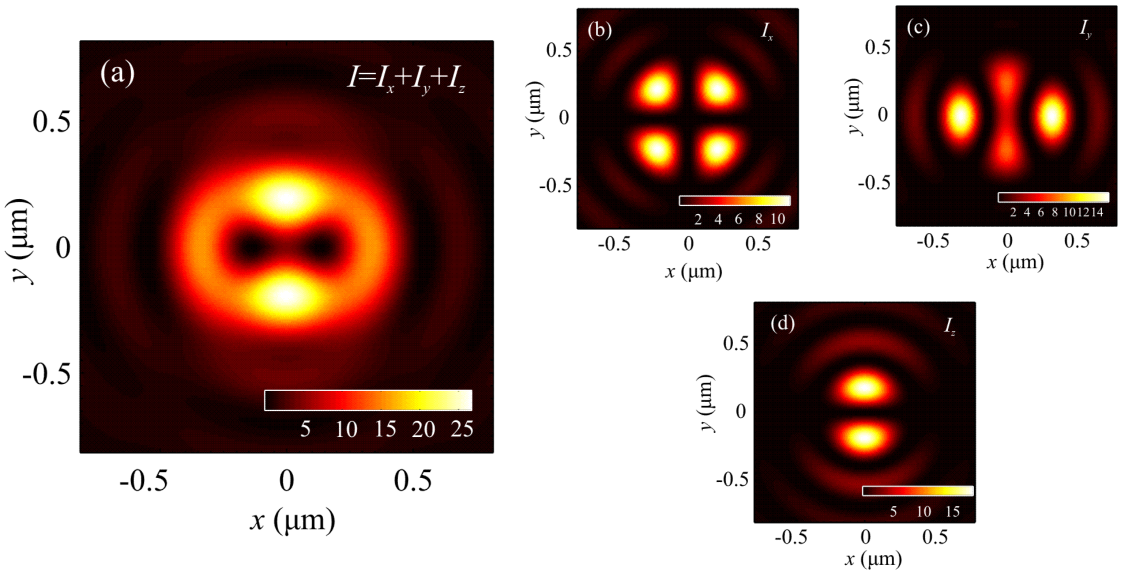

Fig. 2. The total intensity distribution $I = I_x + I_y + I_z$ (a) and the distribution of the intensity components at the focal plane ($z = 0$, $m = 2$): I_x (b), I_y (c) and I_z (d).

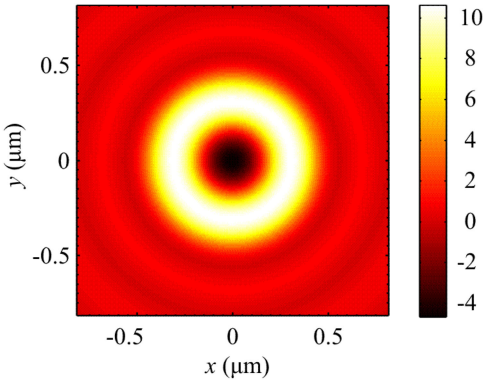

Fig. 3. The distribution of the longitudinal component of the Poynting vector S_z in the focal plane ($z = 0$, $m = 2$).

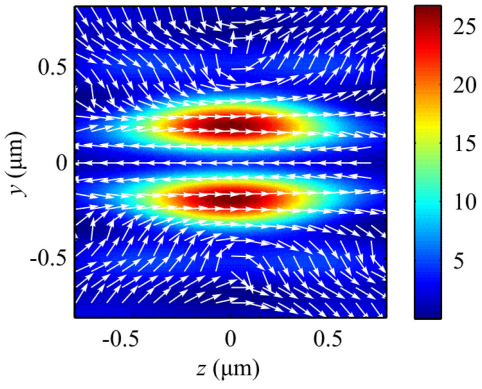

Fig. 4. Intensity pattern I and directions of the Poynting vector S_z (regardless to its absolute value) along the propagation axis of the beam (in the yz plane) for beam of order 2.

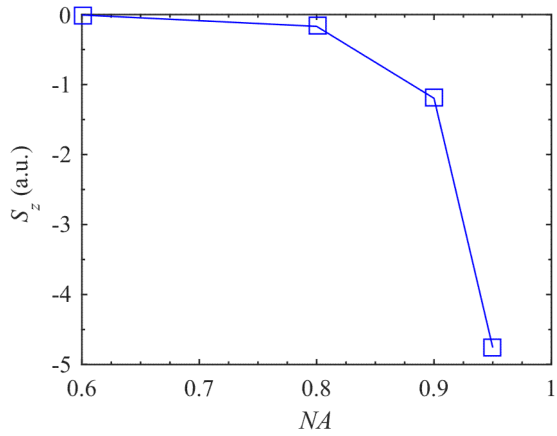

Fig. 5. The dependence of the minimum value of S_z in the center of the focal spot on the numerical aperture NA for an cylindrical vector beams of the order $m = 2$.

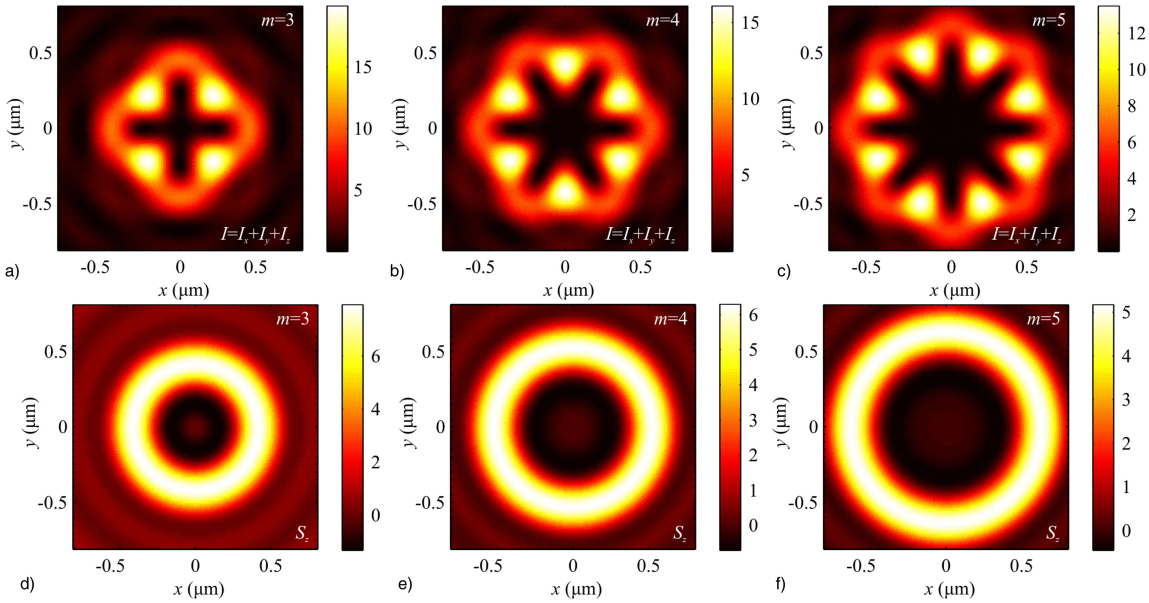

Fig. 6. The intensity distribution (a, b, c) and the longitudinal component of the Poynting vector S_z (d, e, f) in the case of focusing CVB with order $m = 3$ (a, d), $m = 4$ (b, e), $m = 5$ (c, f).

for different orders of cylindrical vector beams (m equals to 1, 2, 3, 4, and 5). Fig. 7c–7e show the intensity distribution and direction of the Poynting vector in the longitudinal plane (zy) for CVB of the third (Fig 7c), forth (Fig 7d), and fifth orders (Fig 7e). It can be seen from Fig. 6 that the intensity distribution has a symmetry of $2(m - 1)$ order. Presence of symmetry with the 4th, the 6th and the 8th order is shown in Fig. 6a, Fig. 6b and Fig 6c respectively. At the same time the energy flow distribution for any m has circular symmetry. This also follows from the expression (9).

From Fig. 7, it could be seen that for the cylindrical vector beam ($m = 1$), there are no negative values of the Poynting vector at the center of the focal spot ($S_z(x = y = 0) = 0$). Reverse energy flow occurs for all m $>$ 1,however, only in the case $m = 2$, the energy backflow is observed at the center of the focal spot ($S_z\,(x = y = 0) < 0$), and it decreases with distance from it. For $m > 2$, the energy flow on the optical axis is zero, however, it increases with increasing distance from the optical axis till gets its maximum and then becomes to decreasing. It shows presence of the reverse flow near the optical axis for $m > 2$, since it looks like a “tube”. Moreover, the width of the negative

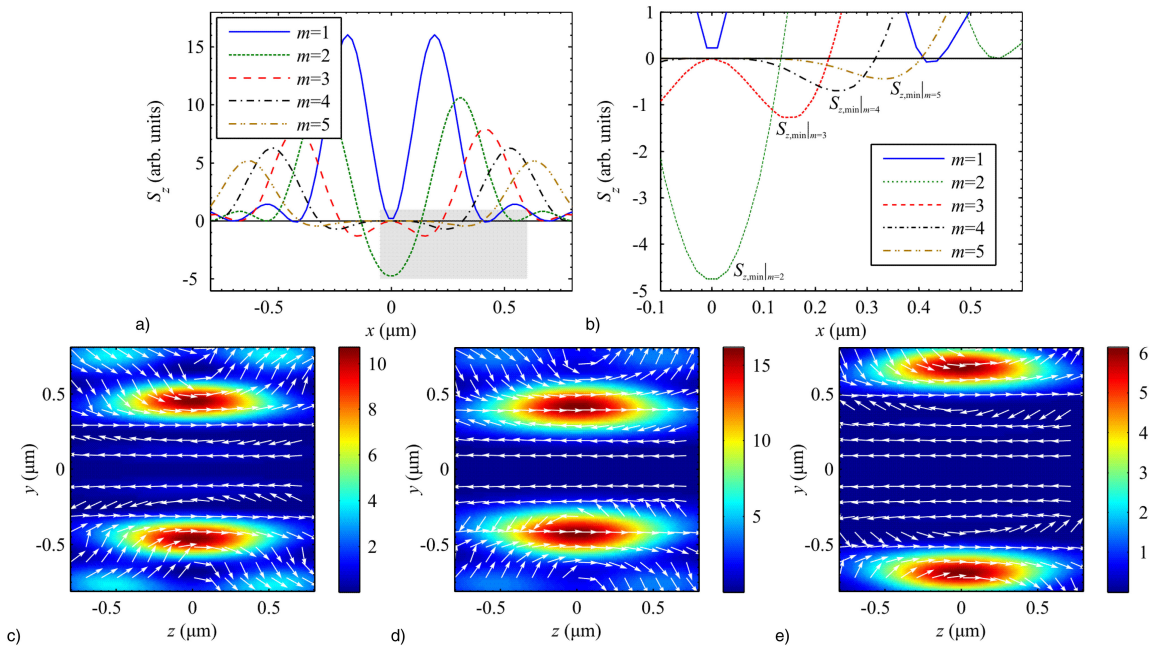

Fig. 7. (a) The distribution of the longitudinal component of the Poynting vector S_z in the focus of the zone plate for the cylindrical vector beams of orders $m = 1$, 2, 3, 4, and 5, (b) the magnified fragment, highlighted on Fig. 7a as gray. Intensity pattern I and directions of the Poynting (regardless to its absolute value) vector S_z along the propagation axis of the beam (in the yz plane) for beams of orders 3 (c), 4 (d), 5 (e).

values region (the diameter of the "tube") increases with increasing m, however the absolute value of energy backflow decreases (Fig. 7b): $|S_{z,\min}(m = 2)| > |S_{z,\min}(m = 3)| > |S_{z,\min}(m = 4)|$

The case for $m = 2$ can be considered as unique, so we focused our research mainly on it.

5. Numerical Simulation Using FDTD-method

The FDTD method was used to verify the results obtained with the Richards-Wolf integrals. The FDTD method implements numerical solution of Maxwell's equations and it has previously established itself as an accurate and reliable method for solving problems of electromagnetic waves propagation [31]. In our investigation we use the FDTD method implemented in the FullWave software (https://www.synopsys.com/optical-solutions/rsoft/passive-device-fullwave.html). Cylindrical vector beam of order $m = 2$ multiplied by the transmission function of the Fresnel zone plate was used as an incident wave in the calculation. In this study, we considered the Fresnel zone plate made of titanium dioxide TiO_2 ($n = 2.67$) with the relief height $h = 0.159$ μm. The radii of zone plate were calculated using the familiar formula $r_m = (m\lambda f + m^2\lambda^2/4)^{1/2}$, where $f = 532$ nm is a focal length (numerical aperture ~1), $\lambda = 532$ nm is a wavelength, m is the radius number. Figure 8 shows the template of a 8 $\times$ 8-μm zone plate. Next parameters of grid for calculated area of 8.6 $\times$ 8.6 $\times$ 1.532 μm were used while simulation by FDTD-method: the grid size was equal to $\lambda/30$, the perfectly matched layers (PML) thickness was 0.5 μm. Simulation results for light focusing are shown in Fig. 9.

It can be seen from Fig. 9 that S_z is negative in the central part of the focal spot ($m = 2$) and has minimum on the optical axis. Thus, the results obtained using two different numerical methods mentioned coincide with each other. The asymmetry of the intensity in Fig. 6a is caused by the a non-radially symmetric template of zone plate.

Fig. 8. Template of the zone plate: black rings – phase of π, white rings – phase of zero.

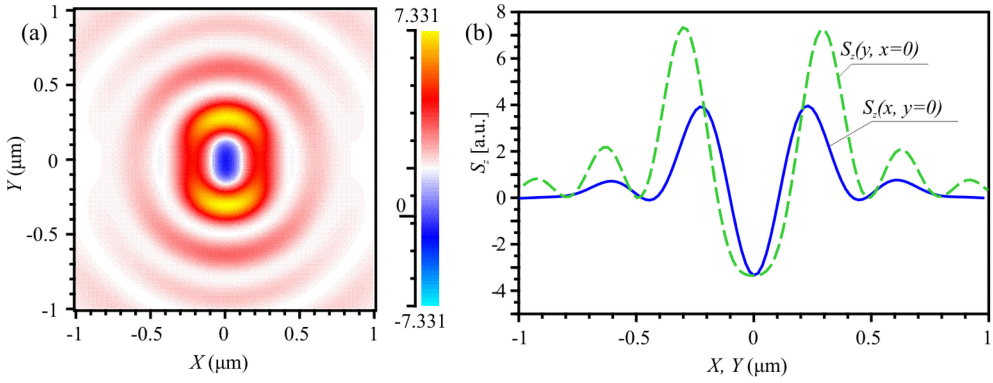

Fig. 9. (a) The longitudinal component of the Poynting vector S_z at the focus of the zone plate, and (b) its sections along *x*- (blue curve) and *y*-axis (green curve).

6. Conclusions

In this paper, tight focusing of high-order cylindrical vector beams was investigated. It was shown theoretically and numerically that in the focus, there are regions with Poynting vectors with directions opposite to the propagation direction of the beam, and the negative values are comparable in absolute value with positive values. If the beam order is equal to two, then the region with negative values of the projection of the Poynting vector is located in the center of the focal spot.

The possibility of obtaining focal spots with the Poynting vector opposite to the direction of beam propagation was previously shown in [24]–[26]; however, in these papers, optical vortices were focused and the energy flow has a spiral shape (spiral reverse flow). In this paper, the reverse flow has a non-vortex character. It also could be noted that a cylindrical vector beam of the second order can be obtained from a linearly polarized beam using a single element that transforms the polarization; for example, a polarizer based on subwavelength gratings [32].

References

[1] Z. Xiaoqiang, C. Ruishan, and W. Anting, "Focusing properties of cylindrical vector vortex beams," *Opt. Commun.*, vol. 414, pp. 10–15, 2018.
[2] Y. Han *et al.*, "Orbital angular momentum transition of light using a cylindrical vector beam," *Opt. Lett.*, vol. 43, pp. 2146–2149, 2018.
[3] S. Matsusaka, Y. Kozawa, and S. Sato, "Micro-hole drilling by tightly focused vector beams," *Opt. Lett.*, vol. 43, pp. 1542–1545, 2018.
[4] P. Pradhan, M. Sharma, and B. Ung, "Generation of perfect cylindrical vector beams with complete control over the ring width and ring diameter," *IEEE Photon. J.*, vol. 10, no. 1, 2018, Art. no. 6500310.
[5] M. Yoshida, Y. Kozawa, and S. Sato, "Subtraction imaging by the combination of higher-order vector beams for enhanced spatial resolution," *Opt. Lett.*, vol. 44, no. 4, pp. 883–886, 2019.

[6] H. Moradi, V. Shahabadi, E. Madadi, E. Karimi, and F. Hajizadeh, "Efficient optical trapping with cylindrical vector beams," *Opt. Exp.*, vol. 27, no. 5, pp. 7266–7276, 2019.
[7] M. Lax, W. Louisell, and W. B. McKnight, "From Maxwell to paraxial wave optics," *Phys. Rev. A*, vol. 11, pp. 1365–1370, 1975.
[8] J. F. Nye, "Polarization effects in the diffraction of electromagnetic waves: The role of disclinations," *Proc. R Soc. Lond. A*, vol. 387, pp. 105–132, 1983.
[9] J. V. Hajnal, "Singularities in the transverse field of electromagnetic waves. I. Theory," *Proc. R. Soc. Lond. A, Math. Phys. Sci.*, vol. 414, pp. 433–446, 1987.
[10] K. S. Youngworth and T. G. Brown, "Focusing of high numerical aperture cylindrical-vector beams," *Opt. Exp.*, vol. 7, pp. 77–87, 2000.
[11] Q. Zhan, "Cylindrical vector beams: From mathematical concepts to applications," *Adv. Opt. Photon.*, vol. 1, pp. 1–57, 2009.
[12] M. Rashid, O. M. Marago, and P. H. Jones, "Focusing of high order cylindrical vector beams," *J. Opt. A, Pure Appl. Opt.*, vol. 11, 2009, Art. no. 065204.
[13] K. Huang, P. Shi, G. W. Cao, K. Li, X. B. Zhang, and Y. P. Li, "Vector-vortex Bessel–Gauss beams and their tightly focusing properties," *Opt. Lett.*, vol. 36, no. 6, pp. 888–890, 2011.
[14] H. Guo, G. Sui, X. Weng, X. Dong, Q. Hu, and S. Zhuang, "Control of the multifocal properties of composite vector beams in tightly focusing systems," *Opt. Exp.*, vol. 19, no. 24, pp. 24067–24077, 2011.
[15] S. Vyas, M. Niwa, Y. Kozawa, and S. Sato, "Diffractive properties of obstructed vector Laguerre–Gaussian beam under tight focusing condition," *J. Opt. Soc. Amer. A*, vol. 28, no. 7, pp. 1387–1394, 2011.
[16] M. Li, S. Yan, Y. Liang, P. Zhang, and B. Yao, "Transverse spinning of particles in highly focused vector vortex beams," *Phys. Rev. A*, vol. 95, no. 5, 2017, Art. no. 053802.
[17] Y. Li, Z. Zhu, X. Wang, L. Gong, M. Wang, and S. Nie, "Propagation evolution of an off-axis high-order cylindrical vector beam," *J. Opt. Soc. Amer. A*, vol. 31, pp. 2356–2361, 2014.
[18] J. Qi *et al.*, "Multiple-slit diffraction of high-polarization-order cylindrical vector beams," *Proc. SPIE,* vol. 10339, 2017, Art. no. 1033927.
[19] X. L. Wang, J. Ding, W. J. Ni, C. S. Guo, and H. T. Wang, "Generation of arbitrary vector beams with a spatial light modulator and a common path interferometric arrangement," *Opt. Lett.*, vol. 32, pp. 3549–3551, 2007.
[20] H. Chen, J. Hao, B. F. Zhang, J. Xu, J. Ding, and H. T. Wang, "Generation of vector beam with space-variant distribution of both polarization and phase," *Opt. Lett.*, vol. 36, pp. 3179–3181, 2011.
[21] Y. Liu *et al.*, "Generation of perfect vortex and vector beams based on Pancharatnam-Berry phase elements,," *Sci. Rep.*, vol. 7, 2017, Art. no. 44096.
[22] S. Sukhov and A. Dogariu, "On the concept of "tractor beams," *Opt. Lett.*, vol. 35, pp. 3847–3849, 2010.
[23] B. Richards and E. Wolf, "Electromagnetic diffraction in optical systems, II. Structure of the image field in an aplanatic system," *Proc. Roy. Soc. A*, vol. 253, pp. 358–379, 1959.
[24] V. V. Kotlyar and A. G. Nalimov, "A vector optical vortex generated and focused using a metalens," *Comput. Opt.*, vol. 41, pp. 645–654, 2017.
[25] S. S. Stafeev and A. G. Nalimov, "Longitudinal component of the Poynting vector of a tightly focused optical vortex with circular polarization," *Comput. Opt.*, vol. 42, pp. 190–196, 2018.
[26] A. Kovalev, V. Kotlyar, and A. Nalimov, "Energy density and energy flux in the focus of an optical vortex: Reverse flux of light energy," *Opt. Lett.*, vol. 43, pp. 2921–2924, 2018.
[27] P. B. Monteiro, P. A. M. Neto, and H. M. Nussenzveig, "Angular momentum of focused beams: Beyond the paraxial approximation," *Phys. Rev. A*, vol. 79, 2009, Art. no. 033830.
[28] I. Rondón-Ojeda and F. Soto-Eguibar, "Properties of the Poynting vector for invariant beams: Negative propagation in Weber beams," *Wave Motion*, vol. 78, pp. 176–184, 2018.
[29] Z. Man *et al.*, "Manipulation of the transverse energy flow of azimuthally polarized beam in tight focusing system," *Opt. Commun.*, vol. 431, pp. 174–180, 2018.
[30] N. Davidson and N. Bokor, "High-numerical-aperture focusing of radially polarized doughnut beams with a parabolic mirror and a flat diffractive lens," *Opt. Lett.*, vol. 29, pp. 1318–1320, 2004.
[31] A. Taflove and S. C. Hagness, *Computational Electrodynamics: The Finite-Difference Time-Domain Method*. Norwood, MA, USA: Artech House, 2005.
[32] S. S. Stafeev *et al.*, "Microlens-aided focusing of linearly and azimuthally polarized laser light," *Opt. Exp.*, vol. 24, pp. 29800–29813, 2016.